

## Possible pairing symmetries in SrPtAs with a local lack of inversion center

Jun Goryo,<sup>1,2,\*</sup> Mark H. Fischer,<sup>3</sup> and Manfred Sigrist<sup>1</sup><sup>1</sup>*Institute for Theoretical Physics, ETH Zurich, 8093 Zurich, Switzerland*<sup>2</sup>*Institute of Industrial Science, the University of Tokyo, 153-8505 Tokyo, Japan*<sup>3</sup>*Department of Physics, Cornell University, Ithaca, NY 14850 USA*

(Dated: November 21, 2018)

We discuss possible pairing symmetries in the hexagonal pnictide superconductor SrPtAs. The local lack of inversion symmetry of the two distinct conducting layers in the unit cell results in a special spin-orbit coupling with a staggered structure. We classify the pairing symmetry by the global crystal point group  $D_{3d}$ , and suggest some candidates for the stable state using a tight-binding model with an in-plane, density-density type pairing interaction. We may have some unconventional states like  $s + f$ -wave and a mixture of chiral  $d$ -wave and chiral  $p$ -wave. The spin orbit coupling is larger than the interlayer hopping, and the mixing between spin-singlet and triplet states can be seen in spite of the fact that the system has a global inversion center.

PACS numbers: 74.20.Rp

The relation between crystal structure and pairing symmetry plays an important role in unconventional superconductivity.<sup>1</sup> Pairing states can be categorized with respect to the irreducible representations of the point group of the crystal lattice and do not mix unless they belong to the same representation. Since the Pauli principle requires that the momentum part of singlet and triplet states possess even and odd parity, respectively, their mixing is prohibited in a system with inversion symmetry. Superconductivity in non-centrosymmetric systems, i.e., CePt<sub>3</sub>Si, opens however the possibility of singlet-triplet mixing.<sup>2–4</sup> It plays a key role to explain the puzzling behavior of the observed nuclear spin-lattice relaxation rate  $T_1^{-1}$ .<sup>5</sup> Microscopically, this mixing is caused by an anti-symmetric spin-orbit coupling (SOC).

Recently, possible singlet-triplet mixing in centrosymmetric systems with a local lack of inversion symmetry, such as special crystal lattices or heterostructures, was discussed.<sup>6,7</sup> The recently-discovered hexagonal pnictide superconductor SrPtAs<sup>8</sup> ( $T_c = 2.4K$ ) belongs to the former case of a special crystal structure. The unit cell possess a global inversion center and its point group is  $D_{3d}$ . There are two distinct honeycomb Pt-As layers within the unit cell each of which has no inversion center. LDA calculations revealed that these two layers are conducting with only a small inter-layer hopping, i.e., the system is quasi-two-dimensional (quasi-2D). In addition, a large splitting of the bands due to anti-symmetric spin-orbit coupling (SOC) was seen. The consequences of this local lack of inversion symmetry on magnetic properties of the superconducting phase<sup>9</sup> as well as on electronic phenomena<sup>10</sup> has previously been studied. In this work, we aim at clarifying its role for the pairing symmetry.

Table I shows the classification of the pairing states based on the global symmetry of the crystal  $D_{3d}$ . We assume intra-layer pairing due to the quasi-2D nature of the system, and focus on on-site and nearest-neighbor-site (nn-site) pairing interactions. It is intriguing that in this table both even-parity spin-triplet and odd-parity spin-singlet pairing appear. The reason is that we have

two distinct layers in the unit cell indicated by  $l = 1, 2$ , and we can introduce an odd-parity factor  $(-1)^l$  under the global inversion operation. Multiplying this factor to a certain pair wave function results in even-parity spin-triplet or odd-parity spin-singlet states. Moreover, spin-singlet and triplet states coexist in some irreducible representations, namely  $A_{1g}$ ,  $E_g$ ,  $A_{2u}$  and  $E_u$ . Therefore, mixing of spin-singlet and triplet states becomes possible in these representations despite the parity conservation.

Since there is no experimental information on the pairing symmetry at present, we discuss some potential candidates for the stable symmetry within a simple model. We use a tight-binding description for electrons on the Pt sites with a Hamiltonian consisting of two parts:  $H = H_0 + H_{sc}$ . The first part,  $H_0$ , is the one-body Hamiltonian introduced by Refs. 9 and 10 in order to reproduce the LDA band structure of SrPtAs,

$$H_0 = \sum_{\mathbf{k}, l, l', s, b} \epsilon_{\mathbf{k}l'l'}^{(b)} c_{\mathbf{k}ls}^{(b)\dagger} c_{\mathbf{k}l's}^{(b)} + \sum_{\mathbf{k}, l, s, b} \alpha_b \boldsymbol{\lambda}_{\mathbf{k}l} \cdot \boldsymbol{\sigma}_{ss'} c_{\mathbf{k}ls}^{(b)\dagger} c_{\mathbf{k}l's'}^{(b)}, \quad (1)$$

with

$$\begin{aligned} \epsilon_{\mathbf{k}l'l'}^{(b)} &= (\epsilon_{1\mathbf{k}}^{(b)} - \mu_b) \tau_{ll'}^0 + \text{Re}[\epsilon_{c\mathbf{k}}^{(b)}] \tau_{ll'}^1 + \text{Im}[\epsilon_{c\mathbf{k}}^{(b)*}] \tau_{ll'}^2, \\ \boldsymbol{\lambda}_{\mathbf{k}l} &= (-1)^l \boldsymbol{\lambda}_{\mathbf{k}} = \tau_{ll}^3 \boldsymbol{\lambda}_{\mathbf{k}}, \end{aligned} \quad (2)$$

where  $c_{\mathbf{k}ls}^{(b)}$  ( $c_{\mathbf{k}ls}^{(b)\dagger}$ ) is the annihilation (creation) operator of an electron in the  $b$ -th band ( $b = 1, 2, 3$ ) with crystal momentum  $\mathbf{k}$ , spin  $s$  in the  $l$ -th layer ( $l = 1, 2$ ). In the above equation, we introduced  $\hat{\sigma}^0$  ( $\hat{\tau}^0$ ) and  $\hat{\sigma}^i$  ( $\hat{\tau}^i$ ), the unit and Pauli matrices acting on the spin (layer) space. Including Pt nearest-neighbor hopping within the plane, as well as nearest- and next-nearest-neighbor hopping between the planes, one finds  $\epsilon_{1\mathbf{k}}^{(b)} = t_1^{(b)} \sum_n \cos \mathbf{k} \cdot \mathbf{T}_n + t_{c2}^{(b)} \cos(c\mathbf{k}_z)$ , and  $\epsilon_{c\mathbf{k}}^{(b)} = t_c^{(b)} \cos(k_z c/2) [1 + \exp(-i\mathbf{k} \cdot \mathbf{T}_3) + \exp(i\mathbf{k} \cdot \mathbf{T}_2)]$  with  $\mathbf{T}_1 = (0, a, 0)$ ,  $\mathbf{T}_2 = (\sqrt{3}a/2, -a/2, 0)$ , and  $\mathbf{T}_3 = (-\sqrt{3}a/2, -a/2, 0)$  the in-plane nearest-neighbor bond vectors used in the tight-binding approach ( $a$  and  $c$  are

TABLE I: (a) Spin-singlet, and (b) spin-triplet basis gap functions. This classification is based on  $D_{3d}$  symmetry. The index  $l = 1, 2$  denotes two distinct layers. The definitions for functions of crystal momentum  $\mathbf{k}$  are,  $e_{\mathbf{k}} \equiv \sum_n \cos \mathbf{k} \cdot \mathbf{T}_n$ ,  $e_{\mathbf{k}}^+ \equiv \sum_n \omega^n \cos \mathbf{k} \cdot \mathbf{T}_n$ ,  $o_{\mathbf{k}} \equiv \sum_n \sin \mathbf{k} \cdot \mathbf{T}_n$ ,  $o_{\mathbf{k}}^+ \equiv \sum_n \omega^n \sin \mathbf{k} \cdot \mathbf{T}_n$ ,  $e_{\mathbf{k}}^- = e_{\mathbf{k}}^{+*}$ ,  $o_{\mathbf{k}}^- = o_{\mathbf{k}}^{+*}$ , where  $\mathbf{T}_{n=1,2,3}$  is the bond vector between nearest-neighbor sites, and  $\omega^n = \exp[2n\pi i/3]$ . Note that we have even-parity spin-triplet part and odd-parity spin-singlet part due to the odd-parity factor  $(-1)^l$ .

$\Gamma$	Parity	(a) spin-singlet $\hat{\Delta}_{\mathbf{kl}}^{\Gamma,m} = i\hat{\sigma}_y \psi_{\mathbf{kl}}^{\Gamma,m}$	(b) spin-triplet $\hat{\Delta}_{\mathbf{kl}}^{\Gamma,m} = i[\hat{\sigma} \cdot \mathbf{d}_{\mathbf{kl}}^{\Gamma,m}] \hat{\sigma}_y$
$A_{1g}$	Even	$\psi_l^{A_{1g}} = 1, \psi_{\mathbf{kl}}^{A_{1g}} = e_{\mathbf{k}}$	$d_{\mathbf{kl}}^{A_{1g}} = (-1)^l o_{\mathbf{k}} \hat{z}$
$A_{2g}$			$d_{\mathbf{kl}}^{A_{2g}} = (-1)^l o_{\mathbf{k}} \hat{x}_{\pm}$
$E_g$		$\psi_{\mathbf{kl}}^{E_g,1} = e_{\mathbf{k}}^+, \psi_{\mathbf{kl}}^{E_g,2} = e_{\mathbf{k}}^-$	$d_{\mathbf{kl}}^{E_g,1} = (-1)^l o_{\mathbf{k}}^+ \hat{z}, d_{\mathbf{kl}}^{E_g,2} = (-1)^l o_{\mathbf{k}}^- \hat{z}$
$A_{1u}$	Odd	$\psi_l^{A_{2u}} = (-1)^l, \psi_{\mathbf{kl}}^{A_{2u}} = (-1)^l e_{\mathbf{k}}$	$d_{\mathbf{kl}}^{A_{1u}} = o_{\mathbf{k}} \hat{x}_{\pm}$
$A_{2u}$			$d_{\mathbf{kl}}^{A_{2u}} = o_{\mathbf{k}} \hat{z}$
$E_u$		$\psi_{\mathbf{kl}}^{E_u,1} = (-1)^l e_{\mathbf{k}}^+, \psi_{\mathbf{kl}}^{E_u,2} = (-1)^l e_{\mathbf{k}}^-$	$d_{\mathbf{kl}}^{E_u,1} = o_{\mathbf{k}}^+ \hat{z}, d_{\mathbf{kl}}^{E_u,2} = o_{\mathbf{k}}^- \hat{z}$

in-plane and inter-layer lattice constants). An important ingredient is the locally anti-symmetric SOC  $\lambda_{\mathbf{kl}}$ , which reads  $\lambda_{\mathbf{k}} = \hat{z} \sum_n \sin \mathbf{k} \cdot \mathbf{T}_n$  for each band. This term is symmetric under global inversion, but anti-symmetric under the local inversion operation in each layer. Due to the Kramers degeneracy, there are only two branches in the energy spectrum of the Hamiltonian (1) for each band

$$\xi_{\mathbf{k}\pm}^{(b)} = \epsilon_{1\mathbf{k}}^{(b)} - \mu_b \pm \sqrt{|\epsilon_{c\mathbf{k}}^{(b)}|^2 + |\alpha_b \lambda_{\mathbf{k}}|^2}. \quad (3)$$

We use tight-binding parameters from Ref. 9 which lead to Fermi surfaces as shown in Fig. 1. With this parameters, the outermost band, labelled band 3, is the dominant band with 74% of the total density of states (DOS) due to its proximity to the van Hove singularity (vHS) at the  $M$  points in the Brillouin zone (BZ). Note that the ratio  $\alpha_b/t_c^{(b)}$ , which parametrizes the effect of the local lack of inversion symmetry, is comparable or larger than 1. This large ratio plays an essential role for the mixing between spin-singlet and spin-triplet state, as we will see below.

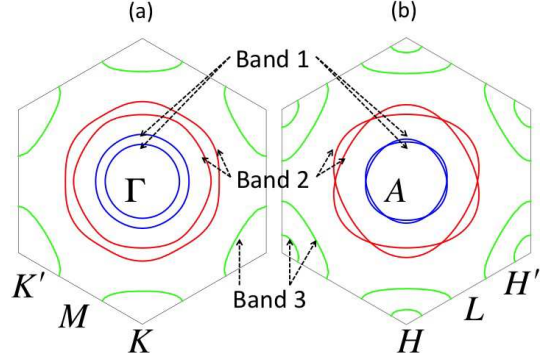


FIG. 1: Fermi surfaces at (a)  $k_z = 0$ , and (b)  $k_z = \pi/c$ . Inner blue, middle red, and outer green lines show the Fermi surfaces for band 1, band 2, and band 3, respectively. Note that there are two branches in each band as suggested in Eq. (3), but one of the branches in band 3 does not cross the Fermi level at  $k_z = 0$ .

with

$$\begin{aligned} V_{s_1 s_2; s_3 s_4}^{bl;l'b'}(\mathbf{k}, \mathbf{k}') &= -g_{\text{on}}^{bb'} \sum_{\Gamma} \psi_l^{(\Gamma)} \psi_{l'}^{(\Gamma)*} (\hat{\sigma}_y)_{s_1 s_2} (\hat{\sigma}_y)_{s_3 s_4} \\ &\quad - g_{\text{nn}}^{bb'} \sum_{\Gamma, m} \psi_{\mathbf{kl}}^{(\Gamma, m)} \psi_{\mathbf{k}'l'}^{(\Gamma, m)*} (\hat{\sigma}_y)_{s_1 s_2} (\hat{\sigma}_y)_{s_3 s_4} \\ &\quad - g_{\text{nn}}^{bb'} \sum_{\Gamma, m} d_{i\mathbf{kl}}^{(\Gamma, m)} d_{j\mathbf{k}'l'}^{(\Gamma, m)*} (\hat{\sigma}_i \hat{\sigma}_y)_{s_1 s_2} (\hat{\sigma}_y \hat{\sigma}_j)_{s_3 s_4}, \end{aligned} \quad (5)$$

For the pairing term  $H_{sc}$  in the total Hamiltonian we assume intra-layer interactions including density-density type attractive interaction, as well as inter-band pair scatterings allowed by the kinematics. Using the basis functions from Table I,  $H_{sc}$  is written in Fourier form as

$$H_{sc} = \sum_{s_1 s_2; s_3 s_4} V_{s_1 s_2; s_3 s_4}^{bl;l'b'}(\mathbf{k}, \mathbf{k}') c_{-\mathbf{k}l s_1}^{(b)\dagger} c_{-\mathbf{k}l s_2}^{(b)\dagger} c_{-\mathbf{k}'l' s_3}^{(b')} c_{\mathbf{k}'l' s_4}^{(b')} \quad (4)$$

where  $g_{\text{on}}^{bb'}$  and  $g_{\text{nn}}^{bb'}$  are the coupling constants for on-site and nearest-neighbor channels. The pairing instability in this model occurs in band 3 with its dominant contribution to the DOS. Smaller gaps then open on the other two bands due to pair scattering.

We solve the linearized gap equation (the eigenvalue

equation for  $T_c$ )

$$\Delta_{s_1 s_2}^{(b)}(\mathbf{k}) = -T_c \sum_{\mathbf{k}', \omega_n} V_{s_1 s_2; s_3 s_4}^{bl; l' b'}(\mathbf{k}, \mathbf{k}') \times [\hat{G}^{(b')}(\mathbf{k}', i\omega_n) \hat{\Delta}^{(b')}(\mathbf{k}') \hat{G}^{(b')}(-\mathbf{k}', -i\omega_n)]_{l' k'}^{s_3 s_4}, \quad (6)$$

where the sum runs over repeated indices, and

$$\hat{G}^{(b)}(\mathbf{k}, i\omega_n) = \left\{ \hat{\sigma}_0 \otimes (i\omega_n \hat{\tau}^0 + \hat{\epsilon}_{\mathbf{k}}^{(b)}) + \alpha_b \boldsymbol{\lambda}_{\mathbf{k}} \cdot \hat{\boldsymbol{\sigma}} \otimes \hat{\tau}^3 \right\}^{-1} \quad (7)$$

is the normal-state Matsubara Green's function. All the possible gap functions are listed as

$$\hat{\Delta}_{\mathbf{kl}}^{(b)\Gamma} = \begin{cases} \hat{\Delta}_{\Gamma}^{(b)}(\psi_l^{\Gamma} + s_{\Gamma}^{(b)} \psi_{\mathbf{kl}}^{\Gamma} + t_{\Gamma}^{(b)} \mathbf{d}_{\mathbf{kl}}^{\Gamma} \cdot \hat{\boldsymbol{\sigma}}) i\hat{\sigma}_y & \Gamma = A_{1g} \\ \Delta_{\Gamma}^{(b)} \mathbf{d}_{\mathbf{kl}}^{\Gamma} \cdot i\hat{\boldsymbol{\sigma}} \hat{\sigma}_y & \Gamma = A_{2g} \\ \sum_m \Delta_{\Gamma, m}^{(b)} (\psi_{\mathbf{kl}}^{\Gamma, m} + t_{\Gamma}^{(b)} \mathbf{d}_{\mathbf{kl}}^{\Gamma, m} \cdot \hat{\boldsymbol{\sigma}}) i\hat{\sigma}_y & \Gamma = E_g \\ \Delta_{\Gamma}^{(b)} \mathbf{d}_{\mathbf{kl}}^{\Gamma} \cdot i\hat{\boldsymbol{\sigma}} \hat{\sigma}_y & \Gamma = A_{1u} \\ \Delta_{\Gamma}^{(b)} (\tilde{s}_{\Gamma}^{(b)} \psi_l^{\Gamma} + s_{\Gamma}^{(b)} \psi_{\mathbf{kl}}^{\Gamma} + \mathbf{d}_{\mathbf{kl}}^{\Gamma} \cdot \hat{\boldsymbol{\sigma}}) i\hat{\sigma}_y & \Gamma = A_{2u} \\ \sum_m \Delta_{\Gamma, m}^{(b)} (s_{\Gamma}^{(b)} \psi_{\mathbf{kl}}^{\Gamma, m} + \mathbf{d}_{\mathbf{kl}}^{\Gamma, m} \cdot \hat{\boldsymbol{\sigma}}) i\hat{\sigma}_y & \Gamma = E_u \end{cases} \quad (8)$$

where  $\Delta_{\Gamma}^{(b)}$  and  $\Delta_{\Gamma, m=1,2}^{(b)}$  are the order parameters, and  $s_{\Gamma}^{(b)}$  and  $t_{\Gamma}^{(b)}$  are the mixing ratios of subdominant spin-singlet and triplet parts, respectively. We see in  $\Gamma = A_{1g}$  and  $A_{2u}$  that there is a mixing between on-site and nearest-neighbor-site pairings, besides the spin-singlet and triplet mixing. We neglect the band dependence of the intra-band couplings, namely,  $g_{\text{on}(\text{nn})} = g_{\text{on}(\text{nn})}^{1,1} = g_{\text{on}(\text{nn})}^{2,2} = g_{\text{on}(\text{nn})}^{3,3}$ , and introduce repulsive inter-band interactions  $g_{\text{on}(\text{nn})}^{1,3} = g_{\text{on}(\text{nn})}^{2,3} = -0.05$ , keeping  $g_{\text{on}(\text{nn})}^{1,2} = 0$ . This choice is motivated by the nesting-like structures between band 2 and 3, and band 1 and 3, respectively.<sup>11</sup> We can then calculate the state with the maximum eigenvalue  $T_c^{\text{max}}$  at a point  $(g_{\text{on}}, g_{\text{nn}})$  in the coupling constant space.

Figure 2 shows the obtained phase diagram. The  $A_{1g}$  state is stabilized when the on-site attraction is dominant, whereas the  $A_{2u}$  state becomes stable in the parameter region where the nn-site attraction is comparable to, or larger than the on-site coupling. From Table I and Eq. (8), we see that both, the  $A_{1g}$  and the  $A_{2u}$  state, have “ $s+f$ ”-wave pairing symmetry, with the  $s$ -wave ( $f$ -wave) component dominant while the  $f$ -wave ( $s$ -wave) component with an odd-parity factor  $(-1)^l$  is subdominant. Therefore, the quasiparticle excitations are fully gapped in the  $A_{1g}$  state, whereas line nodes appear in the  $A_{2u}$  state. The  $A_{2u}$  state invokes a full coherence factor due to the  $s$ -wave component, and would show

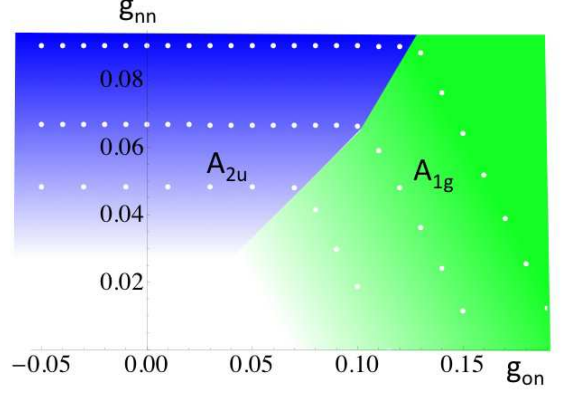


FIG. 2: The phase diagram of the stable pairing states in the coupling constant space  $(g_{\text{on}}, g_{\text{nn}})$ . The tight-binding parameters suggested by LDA calculation<sup>9,10</sup> is used. The sequences of dots show equal  $T_c$  lines at  $T_c/t_1^{(2)} = 10^{-5}, 10^{-4}, 10^{-3}$  from bottom to top.

both Hebel-Slichter peak and power-law type temperature dependence of  $T_1^{-1}$  like CePt<sub>3</sub>Si.<sup>5</sup> The gap structure involves sign changes which give rise to zero-energy Andreev bound states at certain surfaces, e.g. for the normal vector  $[010]$ .<sup>12</sup> Note that the relation of the bound state and topology of the wave function has been discussed in Refs. 13,14. This state belongs to the class AIII of the topological classification<sup>15</sup>.

The locally anti-symmetric SOC introduces a mixing between spin-singlet and triplet parts, which is proportional to

$$\sum_{\mathbf{kl}} \frac{\psi_{\mathbf{kl}}^{\Gamma*} \{ \mathbf{d}_{\mathbf{kl}}^{\Gamma} \cdot \alpha_b \boldsymbol{\lambda}_{\mathbf{k}} \}}{\sqrt{|\epsilon_{c\mathbf{k}}^{(b)}|^2 + \alpha_b^2 \lambda_{\mathbf{k}}^2}} \left( \frac{1}{\xi_{\mathbf{k}+}^{(b)}} \tanh \frac{\xi_{\mathbf{k}+}^{(b)}}{2T_c} - \frac{1}{\xi_{\mathbf{k}-}^{(b)}} \tanh \frac{\xi_{\mathbf{k}-}^{(b)}}{2T_c} \right). \quad (9)$$

This suggests that the mixing is suppressed by a large inter-layer hopping, as expected, since the system has global inversion symmetry and the locally anti-symmetric nature is smeared out when the three dimensionality becomes strong. Such a behavior is also seen in the magnetic susceptibility.<sup>9</sup> In this system, however, the inter-layer hopping has been estimated to be comparable or smaller than the SOC<sup>9,10</sup> and we hence expect a finite value of mixing. Indeed, around the boundary between the  $A_{1g}$  and  $A_{2u}$  phases in Fig. 2, we find enhanced mixing ratios. Their magnitudes are almost band-independent and typical values are  $(s_{A_{1g}}^{(b)}, t_{A_{1g}}^{(b)}) = (-0.51, 0.12)$  in the  $A_{1g}$  phase, and  $(\tilde{s}_{A_{2u}}^{(b)}, s_{A_{2u}}^{(b)}) = (0.15, -0.18)$  in the  $A_{2u}$  phase (definitions of the ratios are given in Eq. (8)).

Figure 3 shows the phase diagram for a shifted chemical potential such that band 3 approaches the vHS. The enhanced DOS naturally leads to reduced coupling constants for the same  $T_c$  as compared to the previous situation. More remarkably, the  $E_g$  state shows up in the

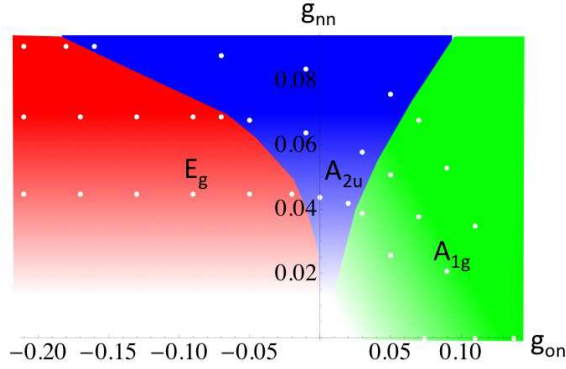


FIG. 3: The phase diagram of the stable pairing state in the coupling constant space ( $g_{on}, g_{nn}$ ) in the DOS enhanced situation, where the Fermi level is located at the vHS point of band 3. The sequences of dots show equal  $T_c$  lines at  $T_c/t_1^{(2)} = 10^{-5}, 10^{-4}, 10^{-3}$  from bottom to top.

region where the on-site coupling is repulsive. One of the reasons for its stability is that the amplitude of the singlet component  $|\psi_{\mathbf{k},l}^{E_g,m}|$  has peaks at the saddle points, which is compatible with the Fermi surface structure. This phase involves two degenerate basis states indicated by  $m = 1, 2$  in Eq. (8), and they make up a Kramers pair. A fourth-order analysis of the Ginzburg-Landau theory yields to degenerate states  $(\Delta_{E_g,1}^{(b)}, \Delta_{E_g,2}^{(b)}) = (1, 0), (0, 1)$ , which both break time-reversal symmetry. We focus here on the first configuration and set  $\Delta_{E_g,2}^{(b)} = 0$ . Expanding the spin-singlet component around the zone-central axes  $k_x = k_y = 0$  gives  $\psi_{\mathbf{k},l}^{E_g,1} = (k_x + ik_y)^2$  with  $d_{x^2-y^2} + id_{xy}$ -wave symmetry, or chiral  $d$ -wave symmetry. Note that  $d_{x^2-y^2}$  and  $d_{xy}$  components are degenerated in the three-fold rotational symmetry. The same expansion for the spin-triplet part yields  $\mathbf{d}_{\mathbf{k},l}^{E_g,1} = (-1)^l(k_x - ik_y)\hat{z}$  with chiral  $p$ -wave symmetry like  $\text{Sr}_2\text{RuO}_4$ .<sup>16</sup> The chiral  $d$ -wave part has  $L_z = +2$ , whereas the chiral  $p$ -wave part  $L_z = -1$  ( $L_z$ :  $z$ -component of the relative angular momentum of the pair). These states can mix

with each other as indicated by Table I.<sup>21</sup> The mixed state is classified into class A in the scheme of the topological classification.<sup>15</sup> Due to the chiral nature of the pairing, this state has a non-zero value for the Chern number defined by the vorticity of the quasiparticle wave function in  $k$  space<sup>17,18</sup> and supports chiral edge states topologically.<sup>19,20</sup>

Our analysis provides insight into the basic trends of the hexagonal superconductor  $\text{SrPtAs}$  whose electrons experience a locally non-centrosymmetric environment. The  $A_{1g}$  state is stable in the electron-phonon coupling limit where on-site attraction is dominant. On the other hand, in the strongly-correlated limit with on-site repulsion or strong nearest-neighbor attraction, the  $A_{2u}$  state is stabilized. In this state, line nodes coming from the spin-triplet component cause a power-law behavior of  $T_1^{-1}$ , whereas a Hebel-Slichter peak arises slightly below  $T_c$  due to the coherence factor of the spin-singlet component, in analogy with  $\text{CePt}_3\text{Si}$ .<sup>5</sup> Such a behavior would be a strong signal of the locally anti-symmetric SOC. As mentioned, the nodal structure results in Andreev bound states at a certain surface,<sup>12</sup> which is related to the topology of the bulk state.<sup>13,14</sup> The  $E_g$  state is possible in some particular cases like DOS enhanced situation owing to the vHS of the saddle points in the hexagonal BZ. This state breaks time-reversal symmetry whose signal could be detected by  $\mu\text{SR}$  measurement for spontaneous magnetization around impurities and also the Kerr rotation experiment, for examples. The state has chirality which is characterized by the Chern number, and leads to topologically-protected chiral edge states.<sup>19,20</sup>

The authors are grateful to D.F. Agterberg, P. Brydon, A. Schnyder and G.-Q. Zheng for stimulating discussions. J.G. is financially supported by a Grant-in-Aid for Scientific Research from Japan Society for the Promotion of Science, Grant No. 23540437 and by Yamada Science Foundation as well as the Pauli Center for Theoretical Studies of ETH Zurich. MHF acknowledges support from NSF Grant DMR-0955822, as well as from NSF Grant DMR-0520404 to the Cornell Center for Materials Research.

\* Electronic address: goryo@phys.ethz.ch

<sup>1</sup> M. Sigrist and K. Ueda, Rev. Mod. Phys. **63**, 239 (1991).

<sup>2</sup> L. P. Gor'kov and E. I. Rashba, Phys. Rev. Lett. **87**, 037004 (2001).

<sup>3</sup> E. Bauer *et al.*, Phys. Rev. Lett. **92**, 027003 (2004).

<sup>4</sup> P. A. Frigeri, D. F. Agterberg, A. Koga, and M. Sigrist, Phys. Rev. Lett. **92**, 097001 (2004).

<sup>5</sup> N. Hayashi, K. Wakabayashi, P. A. Frigeri, and M. Sigrist, Phys. Rev. B **73**, 092508 (2006).

<sup>6</sup> M.H. Fischer, F. Loder, and M. Sigrist, Phys. Rev. B **84**, 184533 (2011).

<sup>7</sup> D. Maruyama, M. Sigrist, and Y. Yanase, J. Phys. Soc. Jpn. **81**, 034702 (2012).

<sup>8</sup> Y. Yoshikubo, K. Kudo, and M. Nohara, J. Phys. Soc. Jpn.

**80**, 055002 (2011).

<sup>9</sup> S. J. Youn, M. H. Fischer, S. H. Rhim, M. Sigrist, and D. F. Agterberg, Phys. Rev. B **85**, 220505 (2012).

<sup>10</sup> S. J. Youn, S. H. Rhim, D. F. Agterberg, M. Weinert, and A. J. Freeman, arXiv:1202.1604

<sup>11</sup> Y. Kamihara, T. Watanabe, M. Hirano and H. Hosono, J. Am. Chem. Soc. **130**, 3296 (2008); I.I. Mazin and J. Schmalian, Physica C **469**, 614 (2009).

<sup>12</sup> S. Kashiwaya and Y. Tanaka, Rep. Prog. Phys. **63**, 1641 (2000).

<sup>13</sup> M. Sato, Y. Tanaka, K. Yada, and T. Yokoyama, Phys. Rev. B **83**, 224511 (2011).

<sup>14</sup> A. P. Schnyder and S. Ryu, Phys. Rev. B **84**, 060504R (2011).

- <sup>15</sup> A. P. Schnyder, S. Ryu, A. Furusaki, and A. W. W. Ludwig, Phys. Rev. B **78**, 195125 (2008).
- <sup>16</sup> A. P. Mackenzie and Y. Maeno, Rev. Mod. Phys. **75**, 657 (2003), and references therein.
- <sup>17</sup> D. J. Thouless, M. Kohmoto, M. P. Nightingale, and M. den Nijs, Phys. Rev. Lett. **49**, 405 (1982).
- <sup>18</sup> M. Kohmoto, Ann. Phys. (N.Y.) **160**, 355 (1985).
- <sup>19</sup> G. E. Volovik, JETP Letters **66**, 522 (1997).
- <sup>20</sup> N. Read and D. Green, Phys. Rev. B **61**, 10267 (2000).
- <sup>21</sup> Indeed, the eigenvalues for the three-fold rotation  $e^{2\pi i L_z/3}$  are the same.